

The $\text{H}_2^+ + \text{He}$ proton transfer reaction: quantum reactive differential cross sections linked with velocity mappings

Mario Hernández Vera,¹ R. Wester,¹ and F. A. Gianturco^{1, a)}

*Institut für Ionenphysik und Angewandte Physik, Universität Innsbruck,
Technikerstr.25/3, A-6020, Innsbruck, Austria.*

(Dated: 14 February 2022)

We construct the velocity map images of the proton transfer reaction between helium and molecular hydrogen ions H_2^+ . We perform simulations of imaging experiments at one representative total collision energy taking into account the inherent aberrations of the velocity mapping in order to explore the feasibility of direct comparisons between theory and future experiments planned in our laboratory. The asymptotic angular distributions of the fragments in a 3D velocity space is determined from the quantum state-to-state differential reactive cross sections and reaction probabilities which are computed by using the time-independent coupled channel hyperspherical coordinate method. The calculations employ an earlier ab initio potential energy surface computed at the FCI/cc-pVQZ level of theory. The present simulations indicate that the planned experiments would be selective enough to differentiate between product distributions resulting from different initial internal states of the reactants.

^{a)}Electronic mail: francesco.gianturco@uibk.ac.at.

I. INTRODUCTION

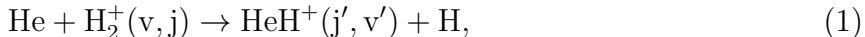
Molecular hydrogen ions (MHIs), in the form of H_2^+ and HD^+ , are considered the simplest molecules in nature. This special characteristic makes them important benchmark systems to test different theories describing their fundamental properties. As members of the family of one-electron molecules, they have enormous potential in ultraprecise spectroscopy^{1,2}, and consequently, they have been proposed as a means to determine the value of fundamental physical constants, to test relativistic quantum mechanics and QED³, or in order to perform the construction of precise molecular clocks⁴. In astrophysics, elemental reactions involving MHIs, like the radiative association between H^+ and H and the proton exchange between HeH^+ and H , are key processes to understand the synthesis of the molecular hydrogen in the early universe⁵. They also provide the essential chemical ingredients for assessing the destruction/survival paths for the HeH^+ molecule in the Interstellar Medium⁶. From the theoretical point of view, investigation of proton exchange reactions have employed frequently H_2 or H_2^+ as models to simplify the quantum calculations. Proton exchange reactions between H_2^+/HD^+ and H or He are part of the reduced group of reactions that can be studied using very accurate Coupled Channel (CC) scattering calculations.

One important reaction that has been investigated extensively during the last few decades is the proton transfer reaction between H_2^+ and He^{7-12} . The former reaction is expected to occur adiabatically up to total energies of about 10 eV, making it a prototype case for comparing theory and experiment. Recently, De Fazio et al.⁷ computed total integral reactive cross section from CC time-independent calculations obtaining good agreement with previous experimental data. Different experiments¹³⁻¹⁷ have demonstrated that the energy stored in the vibrational modes of the *ortho*-hydrogen (o-H_2^+) or *para*-hydrogen (p-H_2^+) molecular ions are more efficient in promoting the reaction than the translational energy. This behaviour has been reproduced by CC calculations⁷ and even by the simpler infinite-order sudden approximation (RIOSAs) treatments¹³. Besides this, we have found no specific calculations using accurate CC reactive approaches that have analysed the angular distributions from the corresponding reactive differential cross sections (DCSs). It is the aim of the present paper to examine in detail just such specific dynamical observables, as we shall discuss below.

Velocity map imaging experiments have proved to be very effective for studying the el-

elementary mechanisms which act in gas-phase ion-molecule reactions. The title reaction is indeed among the most suitable candidates for this kind of experimental analysis owing to the clear mass differences between the charged fragments. The additional and significant advantage of this technique is its capacity of resolving individual reaction products irrespective of their scattering angle or velocity magnitude^{18–20}. It is also possible to employ this method to determine scattering branching ratios which are indeed critical observables for the case of proton exchange reactions involving the HD^+ ion. One should also note here that during the last decade the experimentally achievable intensity of rates of product ions have increased by orders of magnitude, and therefore much more detailed investigations, with better statistical and systematic accuracy for the collected data, can now be performed²¹. However, usually the resolution is not yet sufficient enough to distinguish among the rotational energy spacings appearing between the 3D Newton spheres formed by the products, and the resulting mixture in the velocity space needs to be very carefully unraveled in the ensuing spectra analysis. Therefore, significant numerical simulations of the experiment velocity maps should also realistically include the existing resolution of the crossed-beam imaging data that is determined by the aberration present in the velocity mapping and the actual angular spread of the two reacting beams. This aspect of the experimental situation will therefore be explicitly included in our present numerical simulations in order to better link our computational findings with possible experimental observations.

With regard to the object of the present study, i.e. the proton transfer reaction between H_2^+ and He,



we would like to answer in the main, and among others, the following specific question: Is it possible to distinguish among experimental images of reactions associated with different initial rotational quantum states of the reactants? The collision energy and the initial quantum state of the reactant determine the final angular distributions of the products in the velocity map (VM). Therefore, realistic simulations that would include the intrinsic dispersion of the imaging spectrometer are useful to assess more directly the influence on the final products of the initial conditions in the reaction, and therefore manage to clarify whether or not the effects may be likely to become observable in the experiments. One of the main features which can be an observable in the VM is certainly the variation of the angular distribution of the products. In the case of proton transfer reactions between heavy

+ light-heavy partners, such as $\text{OH}^- + \text{C}_2\text{H}_2$ ²², $\text{NH}_3 + \text{H}_2\text{O}^+/\text{H}_3\text{O}^+$ ^{23,24}, or heavy + light partners $\text{Ar} + \text{H}_2^+$ ²⁵, experimental scattering results reveal distinct forward scattering with little momentum transfer to the ionic product. The above findings thus indicate the presence of a direct stripping mechanism irrespective of the system being studied. On the contrary, for light + light reactions like, $\text{D} + \text{H}_2$ ²⁶ or the ionic reaction considered here, the theory suggests that a large amount of momentum transfer to the products may occur so that backward scattering could be an important effect. Even if the reactive cross-sections can generally be described by using a full quantum treatment, the simpler description of classically impulsive collisions can also help in some cases to qualitatively understand reaction mechanisms.

In the following, we shall therefore simulate the experimental velocity images of the products that result from the exchange proton reaction between He and H_2^+ which will be considered to be in different initial quantum states, aiming at identifying reaction mechanisms that could be directly observed in the real imaging experiments which are currently being planned in our laboratory. As already mentioned before, we shall include in the calculations the intrinsic aberration of our spectrometer in order to underline more directly the links between our calculated DCSs and the experiments.

We shall use time-independent CC hyperspherical coordinate method to calculate the quantum mechanical scattering matrix, from which, the state-to-state DCSs and the reaction probabilities are then calculated. The above data are therefore employed to generate the fragment distributions in the velocity space following the procedure that we shall discuss in the following sections. The calculations are based on a highly correlated reactive potential energy surface (PES) computed with FCI/cc-pVQZ level of quantum chemical theory²⁷ which we shall also briefly outline in the following section.

This paper is structured as follows: In Section II, we provide an outline of the methodology that we have employed to compute the time-independent Scattering Matrix and the ensuing angle-dependent ingredients, i.e. the DCSs from which we shall construct the velocity maps. In the following Section III, we will discuss the outcomes from our reactive quantum scattering calculations and then we will analyze the results of our simulations once the angular distributions are presented in the format of the experimentally observable velocity maps. The conclusions will be reported in the last Section IV.

II. METHODS FOR CALCULATIONS: AN OUTLINE.

A. Quantum reactive scattering calculations

In this work, quantum scattering calculations were performed by using the standard version of the ABC code²⁸. The ABC program employs a time-independent coupled channel hyperspherical coordinate method to calculate the quantum mechanical scattering matrix. The set of coupled hyperradial equations is solved using a logarithmic derivative method. The output of the code are the parity-adapted S -matrix elements $S_{v'j'K',vjK}^{J,P}(E)$ which have to be converted into the standard helicity-representation S -matrix elements $S_{v'j'K',vjK}^J(E)$ ²⁶.

The observables of the reaction can be computed employing the helicity-representation S -matrix elements. The quantum $\text{H}_2^+(v, j) + \text{He} \rightarrow \text{HHe}^+(v', j') + \text{H}$ state-to-state reactive differential cross sections are calculated as,

$$\begin{aligned} & \frac{d\sigma_{v'j'K' \leftarrow vjK}}{d\Omega}(\theta', E) \\ &= \left| \frac{1}{2ik_{vj}} \sum_J (2J+1) d_{K'K}^J(\theta') S_{vjK, v'j'K'}^J(E) \right|^2, \end{aligned} \quad (2)$$

where $d_{K'K}^J(\theta')$ are reduced rotational matrices²⁹, $k_{vj}^2 = 2\mu E/\hbar^2$ and μ is the reduced mass of the initial fragments. J is the value of the total angular momentum quantum number. K and K' are the projection of the total angular momentum vector, \mathbf{J} , on the body-fixed z -axis of reactant and product Jacobi coordinates.

The state-to-state integral reactive cross sections are then defined as

$$\begin{aligned} \sigma_{v'j'K' \leftarrow vjK}(E) &\equiv 2\pi \int_0^\pi d\theta' \sin(\theta') \frac{d\sigma_{vjK, v'j'K'}}{d\Omega} \\ &= \frac{\pi}{k_{vj}^2} \sum_J (2J+1) \left| S_{vjK, v'j'K'}^J(E) \right|^2 \end{aligned} \quad (3)$$

The helicity averaged reaction probability is defined by

$$P_{v'j' \leftarrow vj}(E) = (2j+1)^{-1} \sum_{JKK'} \left| S_{vjK, v'j'K'}^J(E) \right|^2 \quad (4)$$

One can also sum and average over the final and initial helicity quantum numbers to determine the averaged reactive differential cross section,

$$\frac{d\sigma_{j'v' \leftarrow jv}}{d\Omega}(\theta', E) = (2j+1)^{-1} \sum_{KK'} \frac{\sigma_{vjK, v'j'K'}}{d\Omega}(\theta', E) \quad (5)$$

In the present and the following sections we shall omit the arrangement labels from all equations since everything will refer to a single reaction. It is also convenient to refer to the

scattering angle of the molecular product in the center of mass as $\theta = \pi - \theta'$, and therefore we adopt this notation from this point onwards.

B. Velocity map simulations

In our simulation we analyze 30000 reactive collisions in which each fragment follows the probabilities dictated by equations (4) and (5). If the initial collision energy is well defined, then the final velocity of the ion $\text{HeH}^+(j', v')$ is completely determined and it defines a sphere in the velocity space with the origin in the center of mass of the complex HeH_2^+ . The probability for the fragment to end on the surface of such sphere is determined by the state-to-state integral reaction probability given by eq.(4). Then the orientation of the velocity vector is selected from the angular distributions provided by the state-to-state DCS (5).

Once the point is located in the VM, one still has to include the aberrations of the velocity mapping. To characterize the resolution of the electric field configuration, we calculate the radius of the impact position and the time on the detector by means of a Taylor expansion¹⁸,

$$X = \mathbf{D}_X^1|_0 \mathbf{v} + \frac{1}{2} \mathbf{v} \mathbf{D}_X^2|_0 \mathbf{v}^T + \dots, \quad (6)$$

where X denotes either the spatial coordinate R on the detector surface or the time-of-flight to the detector τ . The vector $\mathbf{v} = (r, z, v_r, v_z)$ describes the ion position and velocity before the electric field of the VMI spectrometer is activated³⁰. The points of origin for r and R are located on the symmetry axis setup of our spectrometer¹⁸. The origin for the z -direction is located in the middle between the two lowest plates of the setup, 8 mm above the lowest one. The time-of-flight τ is measured relative to the arrival time of a particle at rest that is starting at $r = 0$ and $z = 0$. $D_X^1(4 \times 1)$ and $D_X^2(4 \times 4)$ represent the respective first and second order matrices of partial derivatives. These matrices were computed for our VMI setup using numerical calculations with SIMION³¹. The matrix entries depend on the mass of the particle for which they are determined.

In the simulations we have considered typical experimental conditions to compute the deviations of the points in the VM. For the proton transfer reaction considered here, the standard deviation of the initial ion energy was 0.1 eV, while the standard deviation of ion angle and the neutral angle are 1.0° and 4.1° , respectively.

C. The reactive potential energy surface.

Here we have used the most recent reactive PES computed for the present reactive system. The details of its evaluation are described extensively in reference²⁷. The surface was obtained at very high level of quantum chemical calculations, using the MRCI approach that included all single and double excitations from the initial CASSCF space. The calculated ab initio points were fitted using the Aguado-Paniagua many-body expansion³² in which the PES of the triatomic system ABC can be expressed as a sum of three monoatomic terms (V_A^1, V_B^1, V_C^1), three 2-body terms ($V_{AB}^2, V_{BC}^2, V_{AC}^2$) and one 3-body term (V_{ABC}^3). The latter term is defined as:

$$V_{ABC}^3(R_{AB}, R_{AC}, R_{BC}) = \sum_{ijk}^M d_{ijk} \rho_{AB}^i \rho_{AC}^j \rho_{BC}^k \quad (7)$$

where the optimal fitting was found by setting the parameter $M = 8$ for those geometries at FCI/cc-pVQZ level of theory. Here M is an order index of the expansion of a product function that decays exponentially with the distance and is defined in the reference. The fitting of the FCI/cc-pVQZ surface turns out to be very accurate and it has been suggested as a promising potential for further dynamics studies²⁷.

The contour plots of the reactive PES as a function of the different Jacobi coordinates are shown in Fig.(1) for reactants and products. The plots evidence the strong anisotropic difference between the interaction of the different fragments, suggesting that the most probable reaction pathway is characterized by linear geometrical configurations in both reactant and product spaces, with H pointing toward the hydrogen atom of HeH^+ when the reaction fragments recede from each other. The PES shape in the reactant space clearly indicates that the “abstraction” mechanism that forms the HeH^+ on the external region of the rotating H_2^+ should be the predominant one in the reaction, as it has also been demonstrated for the inverse reaction³³.

The Reaction (1) turns out to be an endoergic reaction that is quickly promoted by increasing the collision energy above the threshold. We show in Figure 2 the endoergicity of the reactions and all the ro-vibrational levels of $\text{HeH}^+(j', v')$ that are opened at 1.5 eV, the total collision energy used in our simulations. The initial ro-vibrational energy levels considered in this work for the reactants p-H_2^+ and o-H_2^+ are also depicted on that figure. We study only reactions that start with the reactants in the lower excited rotational states, e.g. $j \leq 7$ and $v = 0$. In this situation, the initial kinetic energy of the fragments supplies most

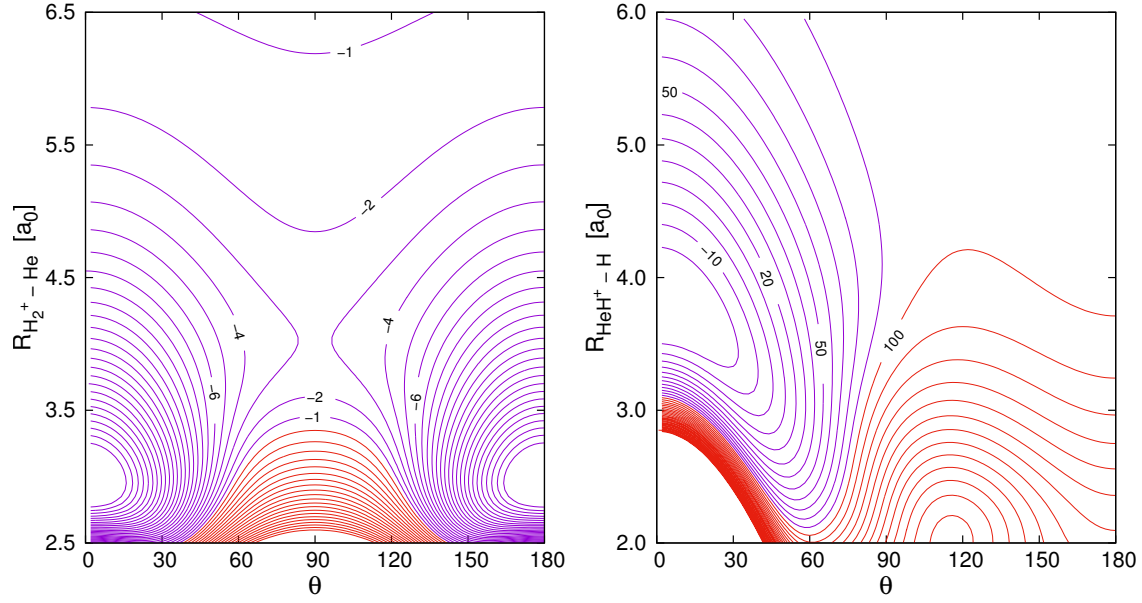


FIG. 1. Contour plot of the PES as a function of the Jacobi coordinates. Energies are in units of 10^2 cm^{-1} and they are measured from the bottom of the asymptotic reactant valley. (a) Contour plot of the reactants' PES constructed by taking the internuclear distance value of H_2^+ at 2.074 au. (b) Contour plot of the products' PES constructed by taking the internuclear distance value of HeH^+ at 1.927 au. In this condition, at $\theta = 0$, the H fragment points toward the hydrogen atom of the HeH^+ molecule.

of the energy for breaking the strong H_2^+ bound and for exciting the internal modes of HeH^+ . The above considerations readily tell us that we can computationally generate the angular distributions of the product molecules by starting with different rotational states of the H_2^+ and therefore observe from the final patterns of such angular distributions possible effects from the internal states of the molecular partners on the outcomes of the reaction, when such internal energy can end up into different rovibrational states of the product molecular ion.

III. COMPUTATIONAL RESULTS: A LINK TO THE EXPERIMENTS

In this section we intend to analyze in some detail reaction (1) in order to unravel its nanoscopic behavior from a computational study of its reactive DCS and from linking such dynamical observables with VM simulations obtained from possible specific experiments.

We have computed the S -matrix of the reaction using the accurate PES presented in

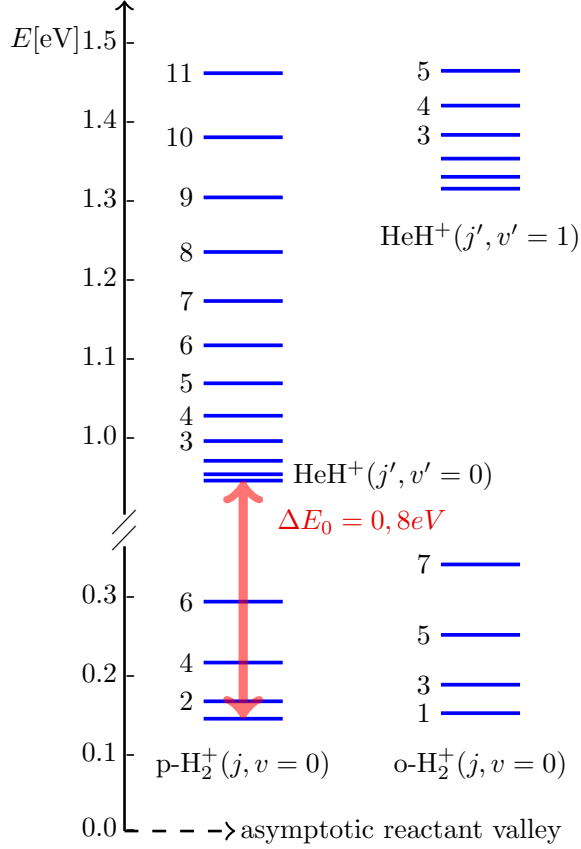


FIG. 2. Schematic description of some energy levels of the reactants and products for the $\text{He} + \text{H}_2^+(v, j) \rightarrow \text{HeH}^+(j', v') + \text{H}$ endoergic reaction.

Section II C and employing the same parameter used in the benchmark work of the De Fazio et. al⁷ However, in contrast with the above mentioned work that analysed the integral cross sections of the reaction, here we focus on the computation of the DCSs and its application in simulating image experiments. The scattering calculations were carried out with the ABC program²⁸ and the input parameters we have employed at 1.2 and 1.5 eV of total collision energies are the following: the total angular momentum quantum number is $J_{totmax} = 54$, the maximum values of the the helicity quantum number is $K_{max} = 12$, the maximum rotational quantum number of any channel is $j_{max} = 26$, the maximum hyperradius is $\rho_{max} = 15 a_0$, and the internal energy in any channel is $e_{max} = 2.3$ eV. The selection of the above total energy values for the present calculations was suggested by the desire to run our numerical modeling under typical conditions of future experimental observations, whereby the endothermic reaction is fully energetically accessible and several cases of different reagents' and products' internal energy distributions could be analyzed.

TABLE I. Total ICS for the reaction $\text{He} + \text{H}_2^+(j, v) \rightarrow \text{HeH}^+ + \text{H}$ as a function of the translational collision energy. Our present results reproduce very closely the state of the art calculations reported in reference⁷ and they are in a good agreement with the recent experimental results¹⁷.

(v, j)	E_c [eV]	$\sigma(vj)$ [\AA^2] (this work)	$\sigma(vj)$ [\AA^2]
0,0	1.357	1.779(-2)	1.776(-2) ^a
1,0	1.085	0.384	0.385 ^a
2,0	0.829	2.051	2.051 ^a
3,0	0.588	4.003	4.008 ^a
0,1	1.350	1.830(-2)	1.909(-2) ^b
1,1	1.079	0.384	0.387 ^b
2,1	0.823	2.019	2.012 ^b
3,1	0.582	3.941	3.975 ^b
4,1	0.355	5.035	5.016 ^b

^a ICS from reference [7] and computed with the RFCI PES (the same PES used in the present work)

^b ICS from reference [7] and computed with the RMRCI PES

Our calculations of the total integral reactive cross sections are in excellent agreement with reference⁷ and with one of the most recent experiment¹⁷. Some of our ICS are presented in table I; they basically reproduce some of the ICSs presented in Figure 2 and 5 of reference⁷. Those authors indicate in their work that they have found better agreement with the existing experiments results for reactions that occur between He and the ion $\text{H}_2^+(v, j = 1)$ in its first $v = 1$ and second $v = 2$ vibrational excited states. However, the disagreement found by the calculations of De Fazio et. al⁷ with the existing experiments for reactions promoted by $\text{H}_2^+(v = 0, j = 1)$ in its ground vibrational state is not as yet completely clear and it may be indicative of uncertainties in the available experiments rather than with problems on the accuracy of the reactive PES. In this work we shall then focus on the reactions between He and the ion H_2^+ ideally prepared in a well defined initial rotational ($j < 7$) and vibrational states ($v = 0$ or $v = 1$).

Following the methods outlined in the previous Section II, we have computed the DCSs for different initial states (and hence relative collision energies) of the reacting molecule and focusing on different internal states of the product polar molecular ion. Some of the results

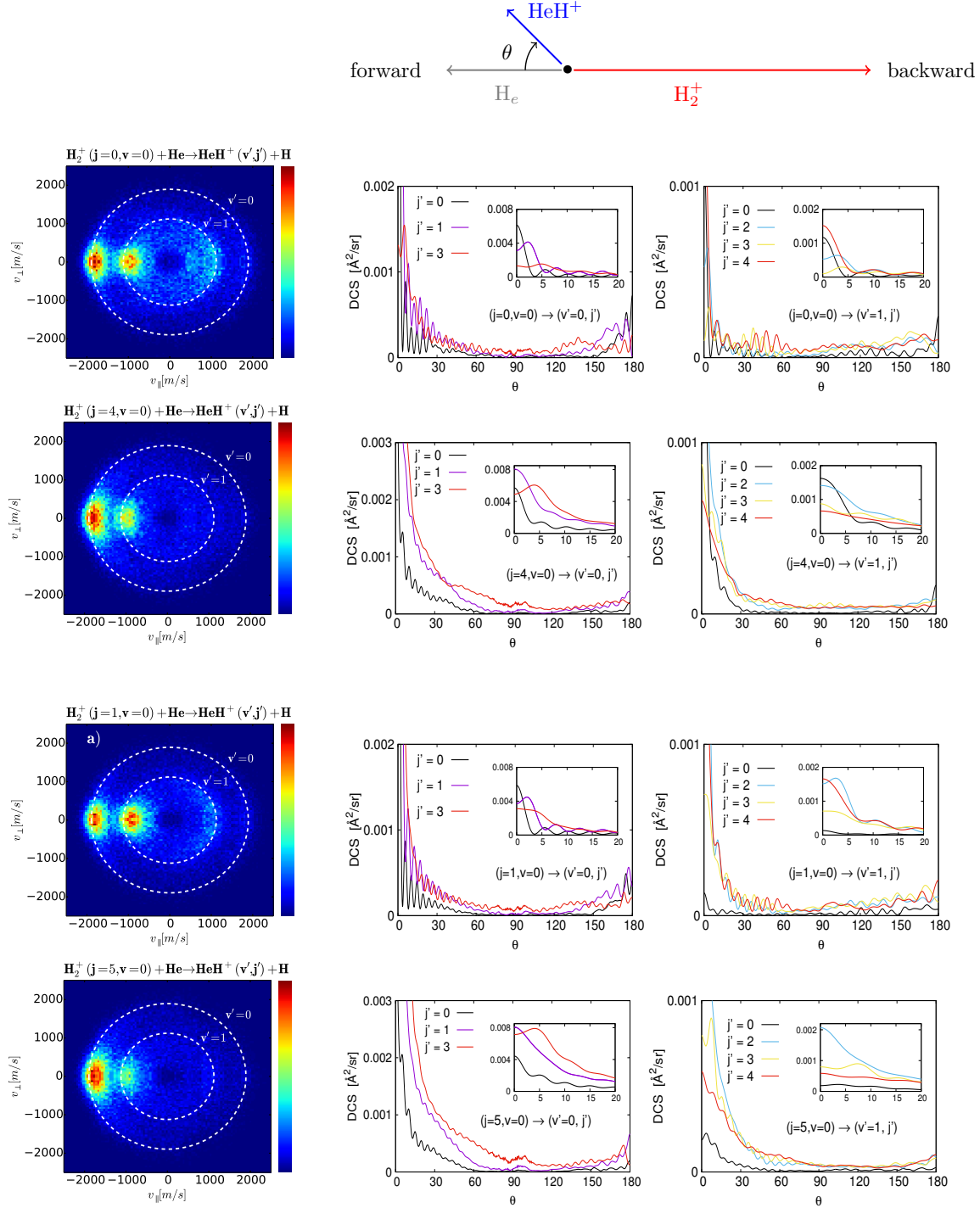


FIG. 3. Velocity map simulation of the experiments and computed DCS for the title reaction at 1.5 eV of total collision energy. The eight panels on the right show some DCSs results while the four panels on the left report the different velocity maps obtained from the same S -matrix calculations. The top panel in this figure reports the products orientation in the velocity map frames.

we have obtained are given in the panels of Figure 3. The following considerations could be a perusal of the many results reported by the panels of Figure 3:

(i) All the DCSs clearly indicate that the reactions have a higher probability of occurring (larger computed values) when the product molecule is obtained in the lower excited rotational states of its ground vibrational level. In fact, the calculations show that there is a clear propensity to produce ions in the lower rotational states with $j' < 5$, while the formation of HeH^+ in a vibrationally excited state is visibly associated with lower reaction probabilities.

(ii) The corresponding velocity maps indicate an additional effect from the reaction dynamics: when molecular products are obtained in the first rotational levels of both $v' = 0$ and $v' = 1$ vibrational states, the reaction is largely producing them in the forward direction. However, when the final ionic product is obtained rotationally excited with $j' > 9$, we found that the backward scattering is promoted.

(iii) The computed angular distributions further show series of rapid oscillations superimposed on the decreasing values of the DCSs as the scattering angle increases. One further sees clearly that such oscillations become much less marked, and with reduced frequencies, when the ionic molecular product is obtained in increasingly higher rotational states.

(iv) The velocity maps also show us that the dominance of the forward scattering peaks is somewhat reduced when the reacting molecular ion initiates the process in an excited rotational level. The data of such maps reported in the 2nd and 4th row of the figure (left-hand-side) indicate that the products are obtained over a larger angular range than when the initial reacting partner molecule is in its lowest rotational state. We shall further discuss this aspect later in this section.

With the intent of unraveling even more the interplay of the molecular internal states with the interaction potential of this system that guides the reactive process analyzed in this work, we report a different presentation of the angular distributions obtained from our calculations in Figure 4.

The top panels of Figure 4 indicate the angular distributions of polar molecular products as the HeH^+ ions are produced in increasingly higher rotational states and when they originate with reactions involving p-H_2^+ partners. The latter are initially in the $j = 4$ state in panel a) while they are in their $j = 6$ state in panel b). At least two clear features can be observed from the angular distributions reported in these panels:

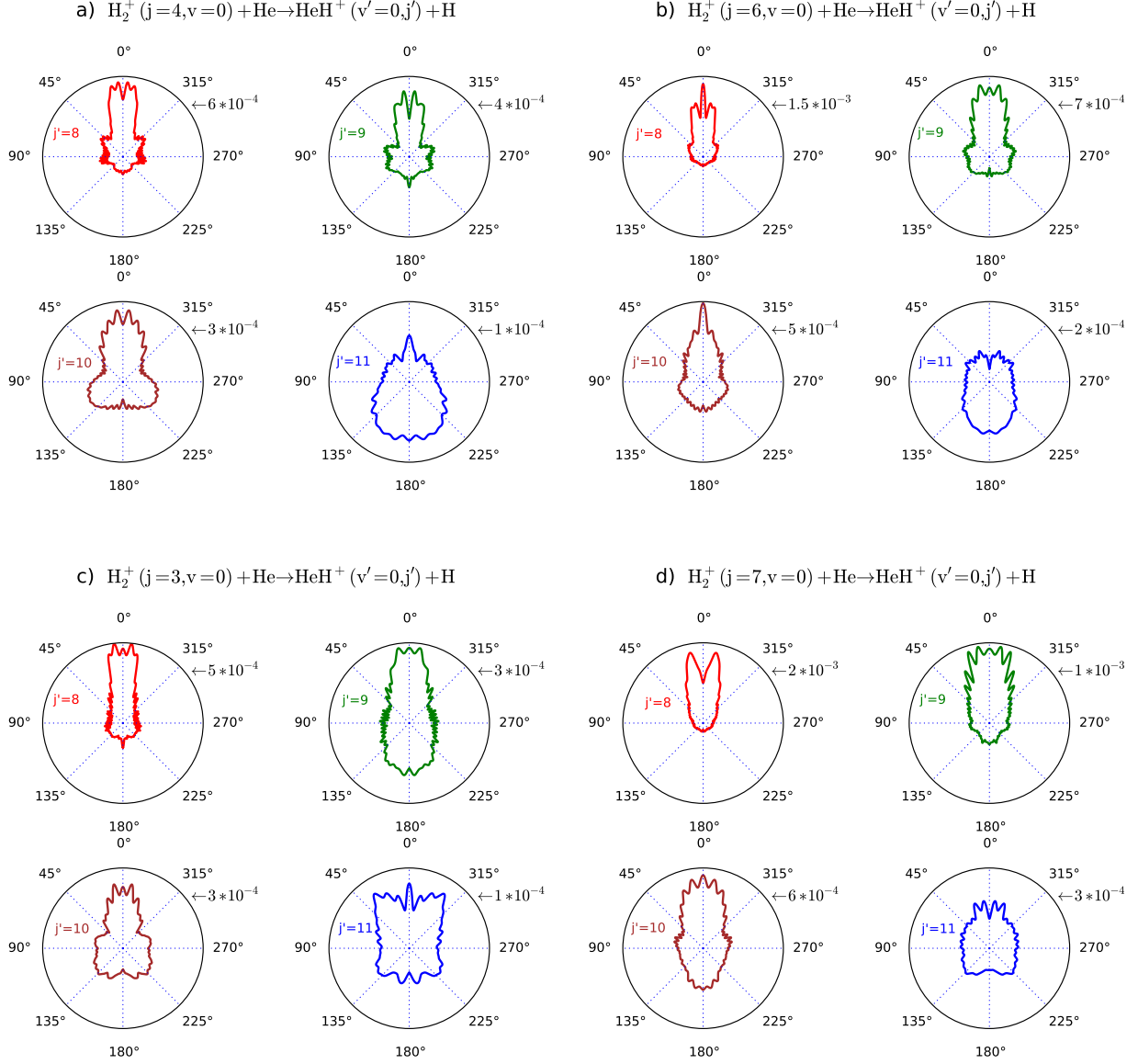


FIG. 4. Polar angular presentation of the product angular distributions for reactions involving p-H_2^+ (panels (a) and (b)) and o-H_2^+ (panels (c) and (d)). The four circular maps in each panel correspond to different final rotational states of the polar molecular product of the present reaction, increasing from left to right and from top to bottom. Each circle in all the panels indicate an upper limit for the specific intensity value of the DCSs for that process. See main text for further details.

(i) The ejection of the products into the backward direction is gradually enhanced as the ionic molecule is produced with higher values of j' . The highest rotational state available at the present collision energy ($j' = 11$) show a dominant ejection of the products into the backward direction.

(ii) all the circular maps in the two panels indicate how sensitive the reaction mechanisms are to the initial quantum states of p-H_2^+ : the maximum values of the DCSs may increase more than a factor of 2 in some directions, while their angular dependence could also become completely altered.

The first of the observed features indicated above can be understood by looking at the relative energy levels reported by Figure 2. The high initial kinetic energy is quickly consumed in the process of breaking the strong chemical bond of H_2^+ ; this effect is favored by a “billiard” effect for this homonuclear molecule. Then if the surplus of energy gets channeled toward the excitation of high rotational states ($j' > 7$) the relative kinetic energy of both product fragments is considerably reduced by about 0.4 eV and therefore the time allowed for the fragments to interact is increased. In addition, there is a second effect: when $j' > 7$, higher values of the relative angular momentum (l') are included in the CC equations. When $l' > 10$ the shape of the ensuing repulsive barrier can make it even more difficult for the product fragments to escape after entering the reaction region, thereby increasing the time of interaction and therefore the angular deflection of the product fragments. The combination of these effects with the strong anisotropic features of the products’ potential interaction (see Figure 1) can therefore strongly alter the balance between backward and forward symmetry of products.

The analysis of the reactions involving o-H_2^+ as the reacting molecular partner (Figure 4.c and 4.d) indicates that the same arguments used for collisions involving p-H_2^+ can be used in this case as well. However, the explanation of the specific differences observed for each state-to-state DCSs of Figure 4 is more complex. The specific differences between state-to-state non-reactive, inelastic DCSs have been explained by the “Fraunhofer theory”³⁴. For reactive collisions, these effects may also be introduced by using statistical treatment based on correlation theory³⁵. The possible application of the above approach will however be attempted in a future, separate publication.

Is it also possible to distinguish among experimental images of reactive collisions between ions prepared in the first initial vibrational excited state $v = 1$ but at different rotational quantum states (see Figure 5). In this situation, the main effect is that the images broaden toward larger values of θ around the forward direction as j increases. The differences between the images is more evident in the region close to the kinematical cut-off where the maximum density of rotational levels for $v' = 0$ are localized. The non-realistic (ideal

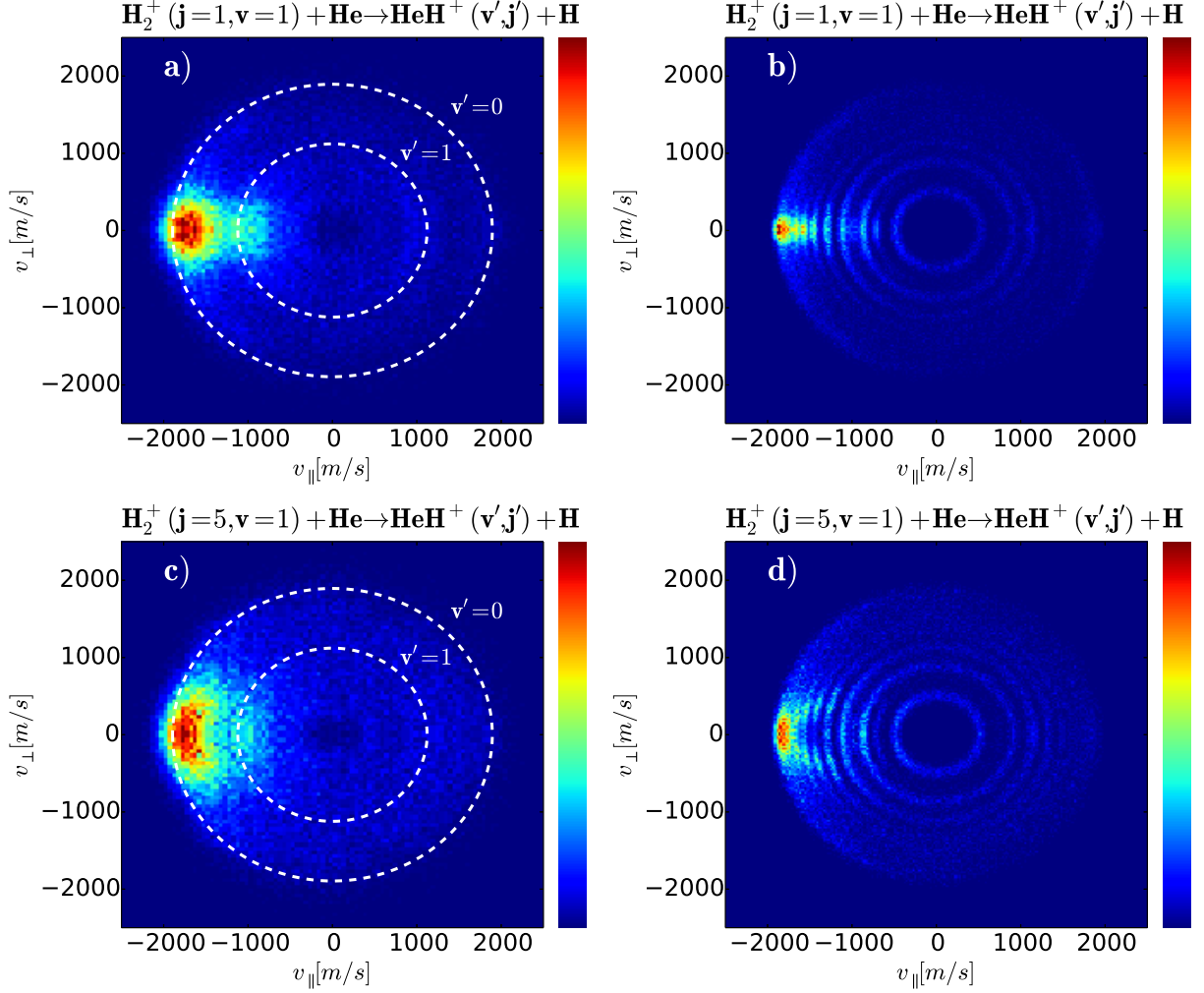


FIG. 5. Simulation of the VM images experiments for the title reaction. The upper panels show the reaction between $\text{o-H}_2^+(\text{v}=1, \text{j}=1)$ and He occurring at 1.08 eV of collision energy. The lower panels show the reaction between $\text{o-H}_2^+(\text{v}=1, \text{j}=5)$ and He occurring at 0.984 eV. In order to disentangle the real simulation presented in Figures a) and c), we display in Figures b) and d) a non-realistic simulation for which the actual standard deviation of every point in the VM is reduced by a factor of 4.

experiments) simulations presented on the right hand side of Figure 5, reveal this effect with more clarity. For reactions that begin with ions in $j=1$, the angular distribution around $\theta=0$ shrinks as j' increases, while the contrary effect is observed for the reactions that start with the reactants in $j=5$. The above effect suggests a more effective transfer of angular momentum in reactions that are promoted by the H_2^+ ions that are already rotationally excited.

There are also variations between images of reactions that occur with the H_2^+ ions in different initial vibrational quantum states but in the same initial rotational states. If one compares, in fact, the reactions between $\text{o-H}_2^+(\text{j} = 1, \text{v})$ and He depicted in the images of Figures 3 and 5, it is possible to observe that the first excited vibrational levels of the products HeH^+ is more easily populated by reactants prepared in the ground vibrational state $v = 0$. Moreover, reactants in the state $|v = 0, j = 1\rangle$ promote more backward scattering than those in the state $|v = 1, j = 1\rangle$. The above finding suggests that the capture of one hydrogen atom by He in the forward direction is less favoured when H_2^+ is in its most stable ground vibrational state. However, the capture mechanism in the forward direction is enhanced by the vibration of H_2^+ that increase the size of the “obstacle” experienced by He and exposes more to the reaction those hydrogen atoms which are away from the molecular equilibrium position. A more rigorous description of this mechanism, however, should take into account a more extensive analysis of the specific features of the reactive PES, the strength of the rotational coupling and the rotational correlations that occur during the reaction.

The mechanism of the reaction can also be understood by finding the preferred direction of attack between the reactants. We have already mentioned in Section II C that the geometrical configuration between He and H_2^+ during initial approach seems to be a key aspect in the reactive process. In an earlier study of ours on the inverse reaction³³, it was suggested that differently rotationally excited reagents could selectively drive the products either through an “abstraction” mechanism or an “insertion” mechanism, with different angular distributions of the corresponding products.

The effects caused on the present reaction by the initial orientation between the fragments can therefore also be studied by performing stereodynamics calculations. In Figure 6 we present the contribution to the total DCSs of two different rotational states of $\text{o-H}_2^+(\text{j} = 1)$ in collisions occurring at 1.07 (6.a and 6.b) and 0.822 (6.c and 6.d) eV of collision energies. Figure (6.a) shows the approach between He and o-H_2^+ in the rotational state described by the helicity quantum number $K = 0$. In this situation, the ion o-H_2^+ has the tendency to be orientated in the same direction of the initial relative velocity vector \mathbf{k} . The reaction is favored in this case by the minimum of the PES in the linear geometrical configuration. Moreover, at the present high collision energy, the efficiency of the reaction is also enhanced by an effective transfer of linear momentum between the three atoms: after the collision with

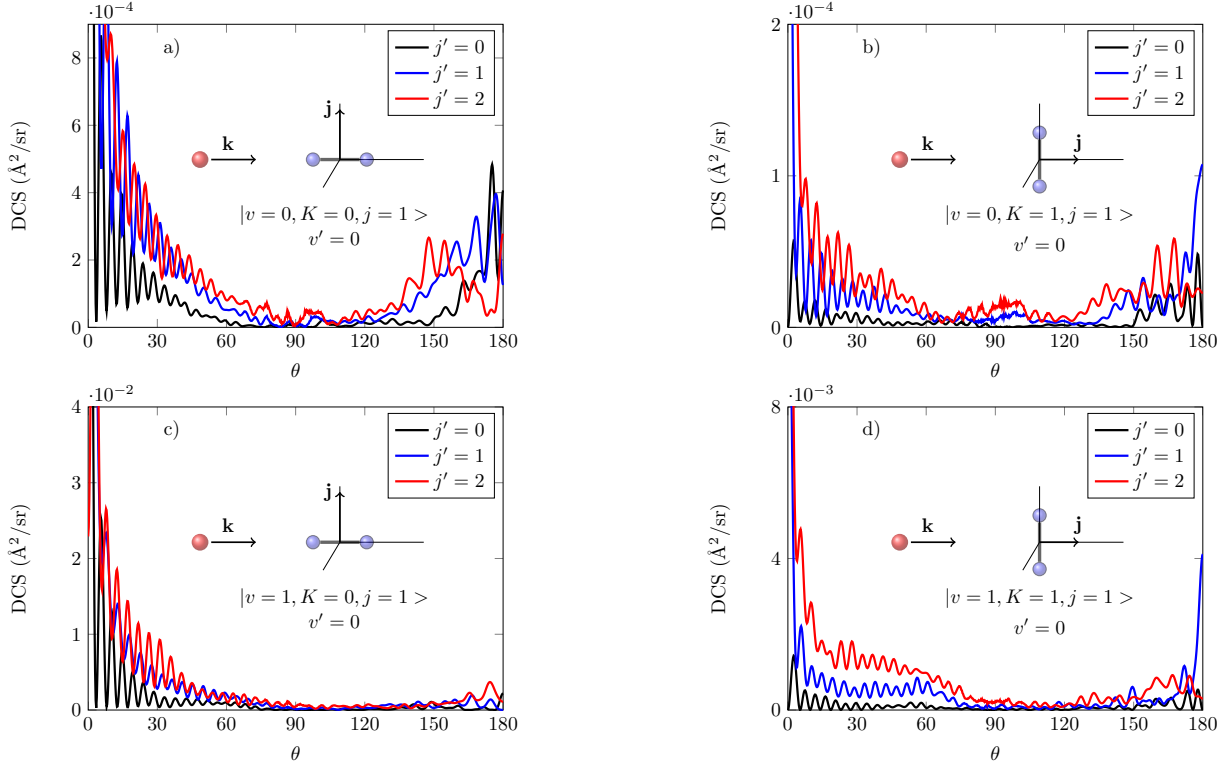


FIG. 6. Stereodynamics calculations of the DCSs for the proton transfer reaction between $\text{H}_2^+(v, j = 1)$ and He. Here we compute the contribution of the initial helicity quantum numbers $K = 0$ and $K = 1$ to the total state-to-state DCSs. The total collision energy is 1.5 eV in all cases.

He, one hydrogen in turn hits back its identical partner, thereby losing most of its extra momentum in the direction of attack. Thus, it becomes more likely to be trapped by the He partner. The second Figure 6.b shows the contribution of the rotational states described by helicity quantum number $K = 1$. In this scenario, the molecule has the propensity to be orientated perpendicularly to the direction of \mathbf{k} , and therefore the helium atom will face in its approach the leading repulsive wall of the T-shape configuration (see Figure 1). This approach is certainly less efficient to promote the reaction and therefore their related reactive DCSs are one order of magnitude lower than those describing the abstraction mechanism in the panel 6.a. Similar ideas may be employed to describe the reactions that occur when the reacting molecular ions are in their first excited vibrational state (Figure 6.c and 6.d). In this case we also observe the reduction of the backward flux, an effect on the reactive scattering that was already described before in this section.

IV. CONCLUSIONS

In this work we have simulated, using ab initio quantum scattering calculations, experimental VM images of the proton transfer reaction between He and H_2^+ . We have found that it is feasible to distinguish among experimental images of reactions associated with different initial rotational (or vibrational) quantum states of the reactants. The experiments might then be able to verify some of the reaction mechanisms predicted by the quantum reactive calculations. The above findings could become experimentally possible as a result of the peculiar angular dependence of the reactive DCSs on the quantum initial states of the reacting molecular ion. We have observed, in fact, that the images of the VM broaden in the forward direction as the initial rotational quantum number of H_2^+ increases, in agreement with the behaviour of the DCSs.

We have further provided in our present discussion a series of qualitative interpretations of this behaviour by linking it to specific features of either the stereodynamics or the length of the times on interaction between reacting partners. From those considerations we were able to observe in the VM simulations that the reactive flux increases into the backward scattering with the decreasing of the initial vibrational quantum numbers of H_2^+ . Finally, we have additionally determined the geometrical configurations of maximal reactivity by performing stereodynamical quantum calculations.

In the future we intend to extend this study to the isotopologue HD^+ in order to assess possibly detectable isotope effects in the reaction with He. In this case, the combination of VM experiments and accurate calculations of the reactive DCSs may reveal new interesting reaction mechanisms, thus providing additional observables like the branching ratio of the reaction between the two available isotopic products.

V. ACKNOWLEDGEMENTS

F.A.G. and R.W. thank the Austrian Science Fund (FWF) for supporting the present research through Project No. P29558-N36. We are also grateful to Björn Bastian and Tim Michaelsen for many illuminating discussions and help on the preparation of the Velocity Map simulations.

REFERENCES

- ¹V. I. Korobov, L. Hilico, and J.-P. Karr, Phys. Rev. Lett. **112**, 103003 (2014).
- ²S. Schiller, I. Kortunov, M. Hernández Vera, F. Gianturco, and H. da Silva, Phys. Rev. A **95**, 043411 (2017).
- ³J. Biesheuvel, J.-P. Karr, L. Hilico, K. S. E. Eikema, W. Ubachs, and J. C. J. Koelemeij, J. Chem. Phys. **7**, 10385 (2016).
- ⁴S. Schiller, D. Bakalov, and V. I. Korobov, Phys. Rev. Lett. **113**, 023004 (2014).
- ⁵W. D. Geppert and M. Larsson, Chem. Rev. **113**, 8872 (2013).
- ⁶S. Bovino, M. Tacconi, F. A. Gianturco, and D. Galli, A&A **529**, A140 (2011).
- ⁷D. D. Fazio, M. de Castro-Vitores, A. Aguado, V. Aquilanti, and S. Cavalli, J. Chem. Phys. **137**, 244306 (2012).
- ⁸S. Kolakkandy, K. Giri, and N. Sathyamurthy, J. Chem. Phys. **136**, 244312 (2012).
- ⁹S. Kumar, H. Kapoor, and N. Sathyamurthy, Chem. Phys. Lett. **289**, 361 (1998).
- ¹⁰S. Mahapatra and N. Sathyamurthy, J. Chem. Phys. **107**, 6621 (1997).
- ¹¹J. Z. Zhang, D. L. Yeager, and W. H. Miller, Chem. Phys. Lett. **173**, 489 (1990).
- ¹²T. Joseph and N. Sathyamurthy, J. Chem. Phys. **86**, 704 (1987).
- ¹³M. Baer, S. Suzuki, K. Tanaka, I. Koyano, H. Nakamura, Z. Herman, and D. J. Kouri, Phys. Rev. A **34**, 1748 (1986).
- ¹⁴D. V. Pijkeren, E. Boltjes, J. V. Eck, and A. Niehaus, Chem. Phys. **91**, 293 (1984).
- ¹⁵J. E. Pollard, J. A. Syage, L. K. Johnson, and R. B. Cohen, J. Chem. Phys. **94**, 8615 (1991).
- ¹⁶J. E. Pollard, L. K. Johnson, and R. B. Cohen, J. Chem. Phys. **95**, 4894 (1991).
- ¹⁷X. N. Tang, H. Xu, T. Zhang, Y. Hou, C. Chang, C. Y. Ng, Y. Chiu, R. A. Dressler, and D. J. Levandier, J. Chem. Phys. **122**, 164301 (2005).
- ¹⁸R. Wester, Phys. Chem. Chem. Phys. **16**, 396 (2014).
- ¹⁹E. Carrascosa, J. Meyer, J. Zhang, M. Stei, T. Michaelsen, W. L. Hase, L. Yang, and R. a. Wester, Nature Communications **8**, 1 (2017).
- ²⁰E. Carrascosa, M. Stei, M. A. Kainz, and R. Wester, Molecular Physics **113**, 3955 (2015).
- ²¹J. Meyer and R. Wester, Annu. Rev. Phys. Chem. **68**, 333 (2017).
- ²²L. Liu, Y. Li, and J. M. Farrar, J. Chem. Phys. **124**, 124317 (2006).
- ²³Y. Li and J. M. Farrar, J. Phys. Chem. A **108**, 9876 (2004).

- ²⁴Y. Li and J. M. Farrar, J. Chem. Phys. **120**, 199 (2004).
- ²⁵T. Michaelson, B. Bastian, E. Carrascosa, J. Meyer, D. H. Parker, and R. Wester, J. Chem. Phys. **147**, 013940 (2017).
- ²⁶J. Z. H. Zhang and W. H. Miller, J. Chem. Phys. **91**, 1528 (1989).
- ²⁷C. Ramachandran, D. De Fazio, S. Cavalli, F. Tarantelli, and V. Aquilanti, Chem. Phys. Lett. **469**, 26 (2009).
- ²⁸D. Skouteris, J. Castillo, and D. Manolopoulos, Comput. Phys. Commun. **133**, 128 (2000).
- ²⁹D. Brink and G. Satchler, *Angular momentum*, 2nd ed. (Oxford University Press, 1968).
- ³⁰A. I. Chichinin, K.-H. Gericke, S. Kauczok, and C. Maul, Int. Rev. Phys. Chem. **28**, 607 (2009).
- ³¹Idaho National Engineering Laboratory, “Simion, version 8.0,” (2006).
- ³²A. Aguado, C. Tablero, and M. Paniagua, **108**, 259 (1998).
- ³³S. Bovino, F. Gianturco, and M. Tacconi, Chem. Phys. Lett. **554**, 47 (2012).
- ³⁴M. Faubel, J. Chem. Phys. **81**, 5559 (1984).
- ³⁵D. A. Case and D. R. Herschbach, Mol. Phys. **100**, 109 (2002).